

Synergistic Effect of Ta₂O₅/F–C Composites for Effective Electrosynthesis of Hydrogen Peroxide from O₂ Reduction^①

WANG Ke^{a, b} PANG Yong-Yu^b XIE Huan^b
SUN Yuan^b CHAI Guo-Liang^{b②}

^a (College of Chemistry and Materials Science, Fujian Normal University, Fuzhou 350007, China)

^b (State Key Laboratory of Structural Chemistry, Fujian Institute of Research on the Structure of Matter, Chinese Academy of Sciences, Fuzhou 350002, China)

ABSTRACT The electrosynthesis of H₂O₂ as an environmentally friendly green process has attracted great attention due to the importance of H₂O₂ in industry and human lives. In this work, a new strategy was proposed to improve the electrical conductivity and H₂O₂ selectivity of transition metal oxides catalysts. F–C (F doped carbon) was coupled with Ta₂O₅ by calcining polyvinylidene fluoride (PVDF) as the carbon source using one step method. The Ta₂O₅/F–C composite catalysts show an excellent H₂O₂ selectivity of more than 80% as well as high reactivity at 2.52 mA/cm², which is greatly enhanced compared to the counterparts of F–C (selectivity of 59%) and Ta₂O₅-800 (current density of 0.85 mA/cm²) in 0.1 M KOH solution. The onset potential for H₂O₂ production on Ta₂O₅/F–C composites is 0.78 V in 0.1 M KOH, which indicates a negligible overpotential. In addition, H₂O₂ selectivity of the catalyst can be stabilized at more than 80% after 10 hours of electrolysis in alkaline electrolyte. The high performance due to the introduction of F–C increases the conductivity of Ta₂O₅ and the synergistic effect between F–C and Ta₂O₅. This work proposed an efficient synergistic effect among F-doped C and Ta₂O₅ for H₂O₂ production.

Keywords: Ta₂O₅/F–C, oxygen reduction reaction, hydrogen peroxide;

DOI: 10.14102/j.cnki.0254–5861.2011–2817

1 INTRODUCTION

Hydrogen peroxide (H₂O₂) is one of the 100 most important chemicals in the world^[1]. Because of its strong oxidative properties and the only by-product is water^[2, 3], H₂O₂ as a green oxidant is often used in almost all chemical industry fields, such as medicine, chemical synthesis, environmental protection, paper bleaching, disinfection, water treatment and so on^[2, 4–7]. So far, 95% of the total H₂O₂ productions annually comes from the anthraquinone process (AO), which contains a multi-step complex process such as hydrogenation over Pd catalyst and rapid oxidation by O₂ to generate H₂O₂^[3, 8–10]. However, such AO process needs complicated steps and several side reactions which cause unnecessary energy consumption^[9, 11]. Secondly, the extremely poor stability of high-concentration H₂O₂ poses

safety hazard and high transportation costs^[12]. Therefore, the development of low-cost and low-concentration H₂O₂ synthesis methods has received increasing attention^[5]. One alternative process is the direct synthesis of H₂O₂ from H₂ and O₂ with a noble metal alloy catalyst^[13–15]. However, this process is not only inefficient but also has a risk of explosion due to the hydrogen-oxygen mixture^[12]. Another alternative is photocatalytic production of hydrogen peroxide from water and dioxygen^[16, 17]. Nevertheless, this method also has the disadvantages of slow kinetics and low efficiency^[1, 2]. Recently, electrosynthesis of H₂O₂ via two-electron O₂ reduction replacing the AO process has caused more and more attention because it is a green process that is efficient, energy-saving and safe^[2, 18].

Due to its low price and abundance, transition metal oxides (such as MnO₂, Co₃O₄, Fe₃O₄, V₂O₅, Ta₂O₅ and so on) have

Received 23 March 2020; accepted 20 April 2020

① This project was supported by the National Natural Science Foundation of China (No. 21703248), and the Strategic Priority Research Program of the Chinese Academy of Sciences (No. XDB20000000)

② Corresponding author. Chai Guo-Liang. E-mail: g.chai@fjirsm.ac.cn

been widely used as an alternative to precious metals in electrocatalytic oxygen reduction reaction (ORR) catalysts^[19–24]. In general, metal oxides show limited ORR performance due to poor electronic conductivity and agglomeration issues^[25].

Ta₂O₅ is currently used as an efficient ORR catalyst due to its high oxygen reduction onset potential (~ 0.95 V vs. SHE) and excellent stability under corrosive environments^[26–28]. However, the limited electronic transport of Ta₂O₅ always reduces its kinetic reaction rate^[29]. Recently, Ta₂O₅ was found to be an efficient catalyst for two electrons ORR to generate H₂O₂^[24, 26]. Carbon supports (such as Vulcan XC72R (V), printex L6 (P)^[22, 30], RGO^[31], carbon black^[32], etc.) show good conductivity and large surface areas have been proved to be helpful to improve the electronic transport and catalytic activity of metal oxides.

Herein, a simple and effective strategy has been proposed to improve the catalytic activity and electronic conductivity of Ta₂O₅ for H₂O₂ electrosynthesis. The polyvinylidene fluoride (PVDF) has been carbonized to high surface area F doped porous carbon and coupled with Ta₂O₅ nanospheres by a simple calcination to generate Ta₂O₅/F–C composite. The Ta₂O₅/F–C composite catalyst presents an excellent performance for H₂O₂ generation with H₂O₂ selectivity and achieves more than 80% and negligible overpotential in 0.1 M KOH alkaline solution, which is greatly enhanced compared to the counterparts of F–C and Ta₂O₅. The enhanced performance was attributed to the synergistic effect between F–C and Ta₂O₅, which increases the conductivity of Ta₂O₅ and improves the selectivity of H₂O₂.

2 EXPERIMENTAL

2.1 Materials

Potassium hydroxide (98.5%) and tantalum powder (99.9%) were bought from Aladdin company. Hydrofluoric acid (40%), nitric acid (65~68%), ammonium hydroxide (25~28%), N-methylpyrrolidone (NMP, 99%), monopotassium phosphate (99.5%) isopropanol (99.7%), glucose (AR) and dipotassium phosphate (99%) were gotten from Sinopharm Chemical Reagent Co. Ltd. PVDF (HSV900) was bought from HeiFei-kejing. Nafion solution (5%) is gotten from Shanghai Hesent Electric Co. Ltd.

2.2 Synthesis of Ta₂O₅ sphere precursor

The Ta₂O₅ sphere precursor was prepared by a co-precipitation process in a typical previous synthesis procedure^[33].

First, 11 mL HF, 22 mL HNO₃ and 77 mL deionized water were mixed and then 1 g tantalum powder was carefully poured into the above solution. Ta powder is completely dissolved after six hours. Finally, a certain amount of ammonium hydroxide was injected to the solution and a white precipitation was generated. The white precipitates were separated, washed with deionized water for three times and then dried in an oven at 60 °C overnight to obtain the final products of Ta₂O₅ nanospheres.

2.3 Synthesis of Ta₂O₅/F–C, Ta₂O₅–800 and F–C

Ta₂O₅/F–C was prepared using one-step process. 0.1 g PVDF and 0.1 g Ta₂O₅ nanospheres were milled with a mortar for 30 minutes, then a certain amount of NMP as a binder was added during the milling process. Such viscous colloids were dried overnight in an oven at 60 °C and then calcinated in a tube furnace at 800 °C for 2 h with a heating rate of 5 °C/min in N₂. Then, they were cooled down to room temperature naturally. The black powders were generated and marked as Ta₂O₅/F–C. As a comparison, PVDF and Ta₂O₅ nanospheres with a mass ratio of 1:2 and 2:1 were also treated with the same process. The products were marked Ta₂O₅/F–0.5C and Ta₂O₅/F–2C, respectively. 0.1 g PVDF was calcinated in a tube furnace at 800 °C for 2 h at a heating rate of 5 °C/min in N₂ and marked as Ta₂O₅–800. 0.1 g Ta₂O₅ nanosphere calcinated in a tube furnace at 800 °C for 2 h with a heating rate of 5 °C/min in N₂ was marked as F–C.

2.4 Structure characterization

The transmission electron microscopy (TEM) images were obtained by using JEOL field-emission microscope (JEOL, Tokyo, Japan) operated at 200 kV. A field emission scanning electron microscope (SEM, FESEM, JSM6700F) equipped with an energy dispersive X-ray spectroscope (EDX, Oxford INCA) is used for acquired SEM images and collecting EDX data (Random five points). X-ray diffraction (XRD) patterns were captured by Miniflex 600 X-ray diffractometer under CuK α radiation. X-ray photoelectron spectroscopy (XPS) was recorded on an ESCALAB 250Xi X-ray photoelectron spectrometer (Thermo Fisher) using monochromatized AlK α radiation (15 kV, 10 mA). The specific surface areas were measured using the Brunauer-Emmett-Teller (BET) model.

2.5 Electrochemical measurements

All electrochemical measurements were performed by an electrochemical workstation (Autolab, PGSTAT302N). Linear sweep voltammetry (LSV) and cyclic voltammetry (CV) experiments were performed using a single cell on a three-electrode system including a platinum gauze as the

counter electrode, a saturated Ag/AgCl electrode as a reference electrode and a rotating ring-disk electrode (RRDE, the areas of ring and disk electrodes are 0.07212 and 0.19625 cm²) as working electrode. The H₂O₂ selectivity was acquired by RRDE experiments in oxygen saturated electrolyte (two electrolytes with pH~8 (phosphate buffered saline) and pH~13 (0.1 M KOH)) at a scan rate of 10 mV/s). 6.0 mg of each catalyst was dispersed in 1.49 mL of water, 0.57 mL of isopropanol, and 0.04 mL of a Nafion solution (5%). The catalyst ink was sonicated for one hour and 16.5 μ L of catalyst ink drop-casted onto the disk electrode and then dried at room temperature. As a comparison, CV and LSV experiments in nitrogen saturated electrolytes were also performed. Electrochemical impedance spectroscopy (EIS) was carried out on a CHI760E working station. Stability test was obtained by a chronoamperometry measurement using RRED under 0.5V vs. RHE with a rotation speed of 1600 rpm for 10 hours. All potentials in this work were converted to reversible hydrogen (RHE) by the following equation (1), H₂O₂ selectivity was calculated by equation (2)^[34], and electronic transfer number was calculated by equation (3)^[5].

$$E_{\text{RHE}} = E_{\text{Ag/AgCl}} + 0.197 + 0.0592 \times \text{pH} \quad (1)$$

$$\text{H}_2\text{O}_2(\%) = \frac{200 \times I_r}{(N \times I_d) + I_r} \quad (2)$$

$$n = \frac{4 \times I_d}{I_d + I_r/N} \quad (3)$$

where I_d is the disk current, I_r the ring current, and N the collection efficiency (0.249).

3 RESULTS AND DISCUSSION

3.1 Structure discussion

The Ta₂O₅/F-C catalyst was successfully synthesized by calcining PVDF and Ta₂O₅ spheres in N₂ at 800 °C. Figs. 1a and S1a show the SEM images with different magnification of the Ta₂O₅ spheres which have a smooth surface and a particle size of tens to hundreds of nanometers. For comparison, the SEM image of Ta₂O₅-800 (Ta₂O₅ spheres were calcined at 800 °C) shown in Fig. S1b suggests that the morphology of Ta₂O₅ sphere maintained after calcination. Figs. 1b and S1c suggest that the F doped C (F-C) displayed as a block shape. Compared with the Ta₂O₅ sphere precursor, the rough surfaces of Ta₂O₅/F-C composite shown in Figs. 1c and S1d illustrate that the F doped C is coupled with Ta₂O₅ sphere. The TEM image of Ta₂O₅ spheres (Fig. 2a) further proves the Ta₂O₅ spheres are dense of several smaller nanospheres, 30~100 nm in size. In Fig. 2b, the TEM structure of F doped C indicates that F-C has a porous layered structure. The TEM image of Ta₂O₅/F-C (Fig. 2c) further suggests that the Ta₂O₅ sphere was coupled with a layer of F doped carbon. Fig. S2a~2c shows the results of five spots EDX data of Ta₂O₅/F-0.5C, Ta₂O₅/F-C and Ta₂O₅/F-2C, illustrating that the composite contains F, O, Ta, and C elements and the atomic ratios of C and Ta are 8:1, 15:1, 31:1, respectively. This corresponds to the feed ratio of Ta₂O₅ spheres and PVDF. Fig. S2d reveals the EDX data of Ta₂O₅-800 draw near to 2:5 which can further prove the presence of Ta₂O₅ phase. The EDX result of F-C (Fig. S2e) shows that the atom ratio of F element is 1.5%.

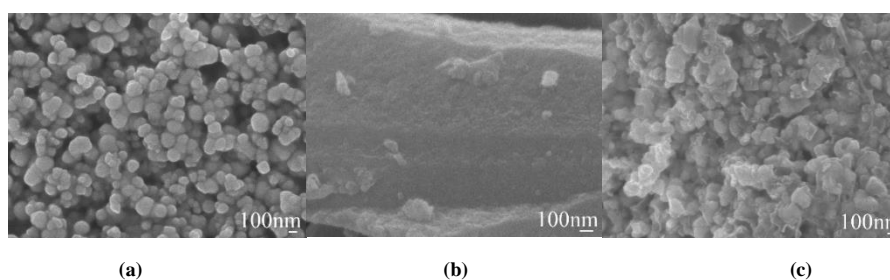


Fig. 1. SEM images of (a) Ta₂O₅ spheres, (b) F doped carbon and (c) Ta₂O₅/F-C

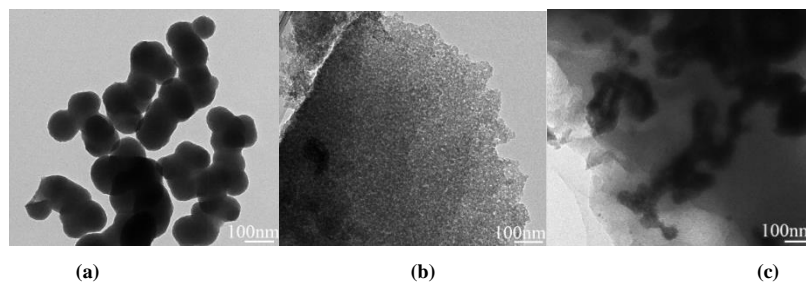


Fig. 2. TEM images of (a) Ta₂O₅ spheres, (b) F doped carbon and (c) Ta₂O₅/F-C

The XRD (X-ray diffraction) patterns of Ta₂O₅ (Fig. S3) before calcination show two wide diffraction peaks, suggesting that Ta₂O₅ spheres synthesized at room temperature are amorphous phase^[35]. The XRD pattern of F-C (in

Fig. S3) shows a wide peak of graphite carbon. The X-ray diffraction (XRD) pattern of Ta₂O₅ and Ta₂O₅/F-C (Fig. 3) mainly demonstrate the orthorhombic pattern of Ta₂O₅ (ICSD No. 25-0922).

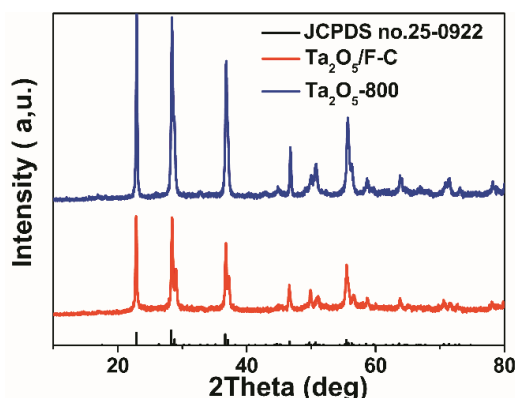


Fig. 3. XRD patterns of Ta₂O₅/F-C and Ta₂O₅-800

The high resolution XPS spectrum for C1s is shown in Fig. 4a, which reveals that the fitting peaks at 284.5, 286.2, 288.2 and 289.8 eV are corresponding to C-C, C-O, C-F and O-C=O chemical bonds, respectively^[36]. It confirmed that F atoms are incorporated into C matrix. The fitting peaks of O 1s spectrum (Fig. 4b) at 531.4, 530.1 and 533.1 eV are corresponding to C=O, O-Ta and O-C=O bonds, which demonstrates that O atoms are combined with C and Ta atoms^[37, 38]. The binding energy of the F 1s peak is 688.9 eV, which corresponds to F-C bond, as shown in Fig. 4c. This further indicates that fluorine is successfully doped into carbon after PVDF carbonization^[36, 37]. The Ta 4f/2 peaks in Fig. 4d are at 26.8 and 28.7 eV, which indicates the presence of Ta₂O₅^[33].

The nitrogen adsorption-desorption isotherms of Ta₂O₅/F-C (Fig. 4e) demonstrate extremely rapid nitrogen

absorption at very low relative pressures, indicating the typical microporosity property of Ta₂O₅/F-C^[39]. In Fig. 4f, the BJH desorption pore-size distribution suggests that the pore width distribution is 1.16 nm. The BET surface area of Ta₂O₅/F-C is 152.6 m²/g and the micropore area is 140 m²/g with a micropore volume of 0.075 cm³/g. However, Ta₂O₅-800 has no conspicuous hysteresis loop at high relative pressure compared to Ta₂O₅/F-C, as shown in Fig. S4. Its BET surface area is only 8 m²/g and the pore volume is insignificant. As a result, it can be deduced that the increased BET surface area and pore volume of Ta₂O₅/F-C mainly comes from piled pore and porous F-C. The increased BET surface area not only exposes more catalytically active sites, but also improves mass transfer. This is more conducive to the production of hydrogen peroxide^[40].

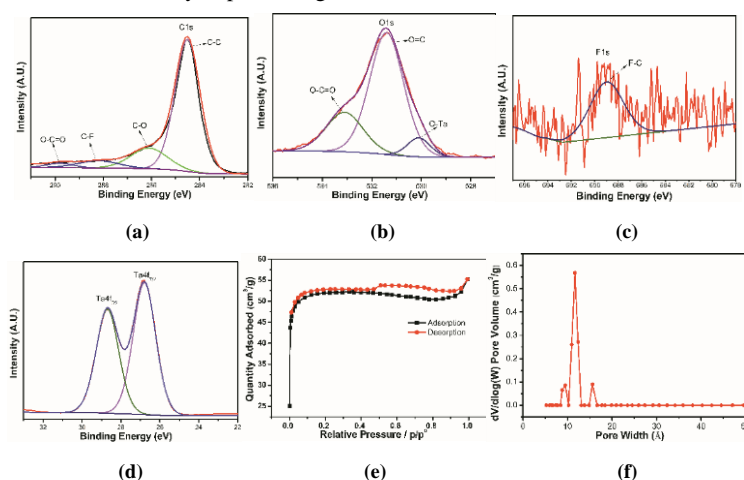


Fig. 4. X-ray photoelectron spectra of (a) C 1s, (b) O 1s, (c) F 1s and (d) Ta 4f for Ta₂O₅/F-C, (e) Nitrogen adsorption-desorption isotherms for Ta₂O₅/F-C and (f) BJH desorption pore-size distribution of Ta₂O₅/F-C

3.2 Electrochemical discussion

The electrochemical performance measurement of the catalysts was based on rotating ring-disk electrode (RRDE) with a rotating speed of 1600 rpm in a three-electrode system. To better evaluate the ORR activity, the ring electrode is made of Pt to oxidize H_2O_2 under a ring potential^[41]. Fig. 5a and 5b reveals the cyclic voltammetry (CV) curves and the linear sweep voltammetry (LSV) profiles of the $\text{Ta}_2\text{O}_5/\text{F}-\text{C}$

composites in N_2 and O_2 saturated alkaline electrolytes (0.1 M KOH solution). A remarkable increase of both the ring and disk currents in the presence of O_2 respect to the N_2 background was observed. The CV curve shows a flat slope in the N_2 saturated solution and an obvious reduction peak under O_2 saturated electrolyte, which indicates the reliability of oxygen reduction performance of $\text{Ta}_2\text{O}_5/\text{F}-\text{C}$.

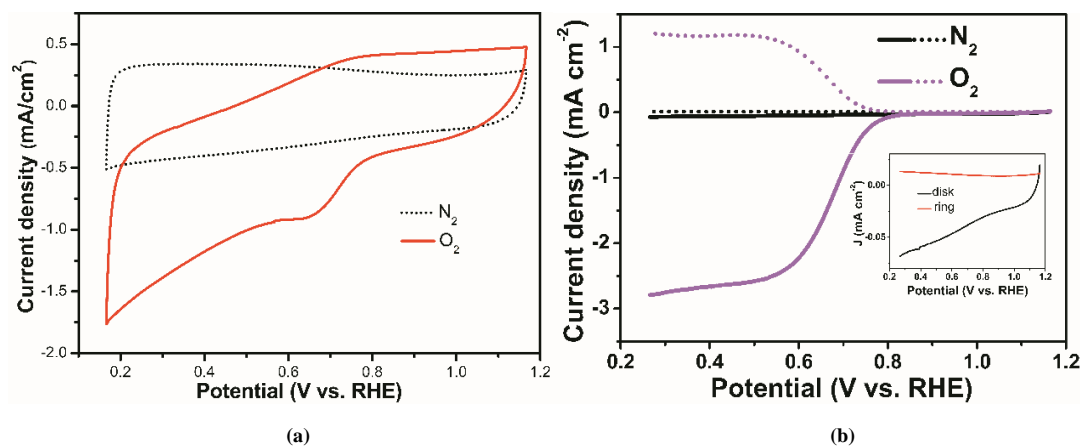


Fig. 5. (a) CV and (b) LSV curves of $\text{Ta}_2\text{O}_5/\text{F}-\text{C}$ in N_2 and O_2 saturated 0.1 M KOH solution

Fig. 6a shows the LSV curves of $\text{Ta}_2\text{O}_5/\text{F}-\text{C}$, $\text{Ta}_2\text{O}_5-800$ and $\text{F}-\text{C}$ in 0.1 M KOH electrolyte. Obviously, the ring current of $\text{Ta}_2\text{O}_5/\text{F}-\text{C}$ is the largest among all the three catalysts. Although $\text{Ta}_2\text{O}_5-800$ has a favorable H_2O_2 selectivity, the oxygen reduction reactivity of $\text{Ta}_2\text{O}_5-800$ is poor. As shown in Fig. 6a and 6b, H_2O_2 selectivity of $\text{Ta}_2\text{O}_5-800$ can reach nearly 70% but the limiting current density is just less than $1 \text{ mA}/\text{cm}^2$ and the onset potential at 0.64 V vs. RHE (defined as the potential at which a current density of $0.1 \text{ mA}/\text{cm}^2$ is achieved). The poor activity of $\text{Ta}_2\text{O}_5-800$ is ascribed to the lower electronic conductivity of Ta_2O_5 ^[25]. As shown in Fig. 6b, the $\text{F}-\text{C}$ has a poor H_2O_2 selectivity about 55%, which is far less than the $\text{Ta}_2\text{O}_5/\text{F}-\text{C}$ (80.8%). The resistance measurement further confirms the enhanced conductivity of the $\text{Ta}_2\text{O}_5/\text{F}-\text{C}$ electrode. The high frequency range of EIS (Fig. S5) illustrated charge transfer ability for $\text{Ta}_2\text{O}_5/\text{F}-\text{C}$ and $\text{Ta}_2\text{O}_5-800$. EIS in high frequency region (100 kHz to 10 Hz) was fitted with an equivalent circuit diagram to get charge transfer resistance. Obviously, the charge transfer resistance of $\text{Ta}_2\text{O}_5-800$ is two orders of magnitude larger than $\text{Ta}_2\text{O}_5/\text{F}-\text{C}$, which indicates the introduction of $\text{F}-\text{C}$ improved the conductivity of Ta_2O_5 successfully.

The LSV profiles of $\text{Ta}_2\text{O}_5/\text{F}-0.5\text{C}$, $\text{Ta}_2\text{O}_5/\text{F}-\text{C}$, and $\text{Ta}_2\text{O}_5/\text{F}-2\text{C}$ that contain different ratios of F are shown in

Fig. S6a. The $\text{Ta}_2\text{O}_5/\text{F}-\text{C}$ displayed the highest disk current and ring current among the three catalysts, demonstrating that $\text{Ta}_2\text{O}_5/\text{F}-\text{C}$ shows an excellent activity for two-electron ORR that is better than $\text{Ta}_2\text{O}_5/\text{F}-\text{C}-0.5$ and $\text{Ta}_2\text{O}_5/\text{F}-\text{C}-2$. The $\text{Ta}_2\text{O}_5/\text{F}-\text{C}$ exhibits a high selectivity of H_2O_2 of 80.8% at 0.49 V vs. RHE , and the selectivity is close to 80% within a wide potential range of $0.25 \sim 0.55 \text{ V}$. This catalyst also displays an excellent oxygen reduction activity with the onset potential of 0.78 V vs. RHE , which shows almost no overpotential. These efficient activity of $\text{Ta}_2\text{O}_5/\text{F}-\text{C}$ surpass those of most other carbon support metal oxides in alkaline media (Table S1). The different selectivity shown in Fig. S6b can illustrate the feed ratio of C and Ta also play a nonnegligible role in the activity of such composites and the feed ratio of 1:1 is optimal. In Fig. 6a, $\text{F}-\text{C}$ shows the largest disk current and the most positive onset potential among all catalysts, but the ring current is lower than $\text{Ta}_2\text{O}_5/\text{F}-\text{C}$. This unusual performance can be explained that the $\text{F}-\text{C}$ tends to take four-electron ORR pathway to generate H_2O . The H_2O_2 selectivity of $\text{Ta}_2\text{O}_5/\text{F}-\text{C}$ is better than that of $\text{F}-\text{C}$ and Ta_2O_5 , which demonstrates that $\text{F}-\text{C}$ and Ta_2O_5 propose a synergistic catalytic effect. Both the ring and disk currents were also obtained by RRDE in a neutral condition (0.1 M PBS solution with $\text{PH} = 8$) for $\text{Ta}_2\text{O}_5/\text{F}-\text{C}$ and $\text{F}-\text{C}$ (Fig. S7a). In Fig. S7b, $\text{Ta}_2\text{O}_5/\text{F}-\text{C}$ shows a considerable performance for

H₂O₂ production with the selectivity of 68.5%, compared with the selectivity of 43.6% for F-C. Figs. 6c and S8 are the Tafel slopes for all the catalysts in different electrolytes. Obviously, Ta₂O₅/F-C has the lowest Tafel slope in alkaline electrolytes, so it shows the best kinetic rate than other catalysts. To evaluate its stability, a constant potential hold stability test at 0.5 V vs. RHE was performed by rotating

ring-disk electrode at 1600 rpm. Fig. 6d shows that the ring and disk current density is rather stable during 10 h electrolysis for Ta₂O₅/F-C. Fig. S9 shows the H₂O₂ selectivity and electron transfer number (ETN) of the catalysts after 10 h electrolysis. The H₂O₂ selectivity kept around 80% and ETN is around 2.3 after electrolysis for 10 h.

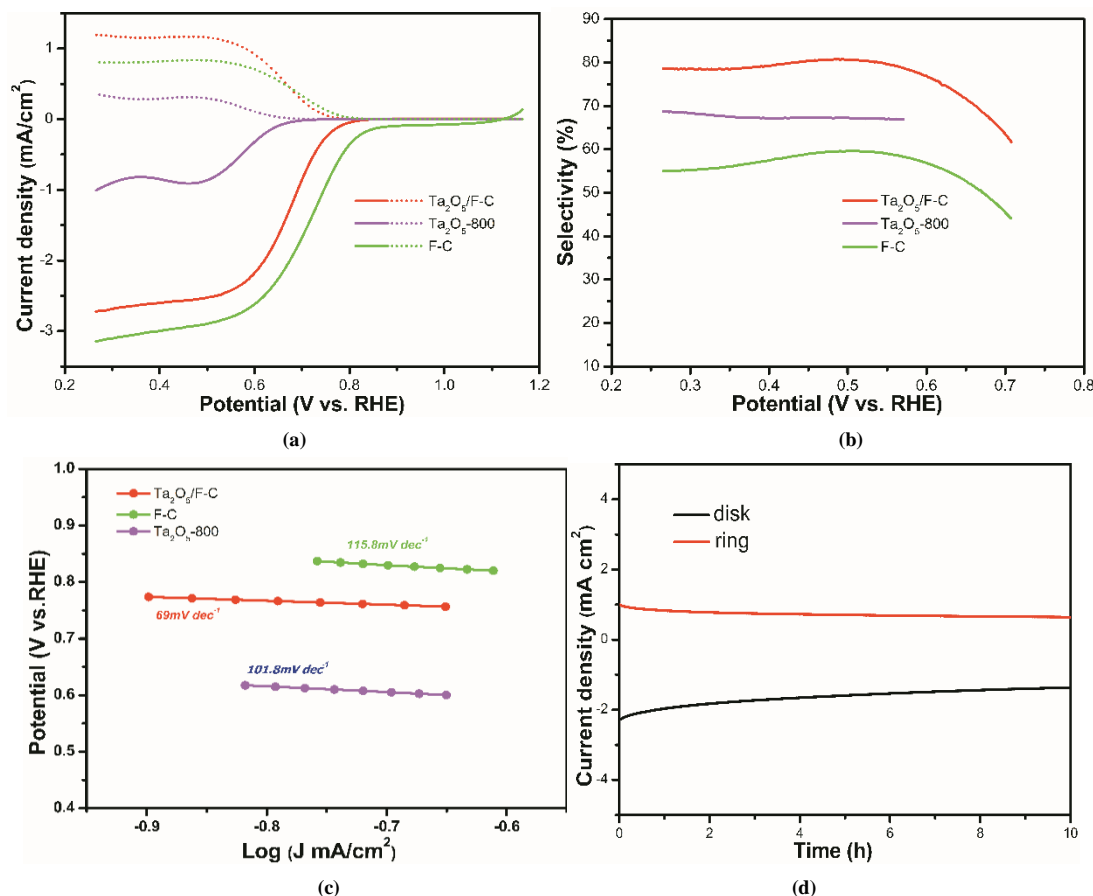


Fig. 6. (a) LSV curves of Ta₂O₅/F-C, Ta₂O₅-800 and F-C (scan rate of 10 mV/s with a rotation speed of 1600 rpm). (b) H₂O₂ selectivity of Ta₂O₅/F-C, Ta₂O₅-800 and F-C in O₂ saturated 0.1 M KOH electrolyte. (c) Tafel slopes for corresponding catalysts in O₂ saturated 0.1 M KOH electrolyte. (d) Stability test for Ta₂O₅/F-C. All plots were subtracted from the nitrogen background current and the pH of test condition is 13

4 CONCLUSION

In summary, a synergistic effect is proposed to enhance the performance of Ta₂O₅/F-C composite catalysts for efficient H₂O₂ electrosynthesis. The electrical conductivity of Ta₂O₅ was significantly increased by forming Ta₂O₅/F-C interface. The Ta₂O₅/F-C catalyst shows an excellent selectivity more

than 80% and long-term stability for H₂O₂ production. The greatly enhanced performance of Ta₂O₅/F-C compared to F-C (selectivity of 59%) Ta₂O₅-800 (current density of 0.85 mA/cm²) counterparts were ascribed to the synergistic effect between F-C and Ta₂O₅. This work could provide a new way to rational design of carbon-supported metal oxide catalysts for H₂O₂ electrosynthesis.

REFERENCES

- (1) Zhou, W.; Meng, X.; Gao, J.; Alshawabkeh, A. N. Hydrogen peroxide generation from O₂ electroreduction for environmental remediation: a state-of-the-art review. *Chemosphere* **2019**, 225, 588–607.
- (2) Campos-Martin, J. M.; Blanco-Brieva, G.; Fierro, J. L. Hydrogen peroxidesynthesis: an outlook beyond the anthraquinone process. *Angew. Chem. Int. Ed.* **2006**, 45, 6962–6984.
- (3) Yi, Y.; Wang, L.; Li, G.; Guo, H. A review on research progress in the direct synthesis of hydrogen peroxide from hydrogen and oxygen: noble-metal catalytic method, fuel-cell method and plasma method. *Catal. Sci. Technol.* **2016**, 6, 1593–1610.
- (4) Droguet, P.; Elmaleh, S.; Rumeau, M.; Bernard, C.; Rambaud, A. Hydrogen peroxide production by water electrolysis: application to disinfection. *J. Appl. Electrochem.* **2001**, 31, 877–882.
- (5) Jiang, Y.; Ni, P.; Chen, C.; Lu, Y.; Yang, P.; Kong, B.; Fisher, A.; Wang, X. Selective electrochemical H₂O₂ production through two-electron oxygen electrochemistry. *Adv. Energy Mater.* **2018**, 8, 180190–9.
- (6) Lane, B. S.; Burgess, K. Metal-catalyzed epoxidations of alkenes with hydrogen peroxide. *Chem. Rev.* **2003**, 103, 2457–2474.
- (7) Pan, Z.; Wang, K.; Wang, Y.; Tsiakaras, P.; Song, S. *In-situ* electrosynthesis of hydrogen peroxide and wastewater treatment application: a novel strategy for graphite felt activation. *Appl. Catal. B-Environ.* **2018**, 237, 392–400.
- (8) García-Serna, J.; Moreno, T.; Biasi, P.; Cocero, M. J.; Mikkola, J. P.; Salmi, T. O. Engineering in direct synthesis of hydrogen peroxide: targets, reactors and guidelines for operational conditions. *Green Chem.* **2014**, 16, 2320–2343.
- (9) Melchionna, M.; Fornasiero, P.; Prato, M. The rise of hydrogen peroxide as the main product by metal-free catalysis in oxygen reductions. *Adv. Mater.* **2019**, 31, 18029–20.
- (10) Yang, S.; Verdager-Casadevall, A.; Amarson, L.; Silvoli, L.; Čolić, V.; Frydendal, R.; Rossmeisl, J.; Chorkendorff, I.; Stephens, I. E. Toward the decentralized electrochemical production of H₂O₂: a focus on the catalysis. *Acs Catal.* **2018**, 8, 4064–4081.
- (11) Perry, S. C.; Pangotra, D.; Vieira, L.; Csepei, L. I.; Sieber, V.; Wang, L.; de León, C. P.; Walsh, F. C. Electrochemical synthesis of hydrogen peroxide from water and oxygen. *Nat. Rev. Chem.* **2019**, 3, 442–458.
- (12) Zhang, J.; Zhang, H.; Cheng, M. J.; Lu, Q. Tailoring the electrochemical production of H₂O₂: strategies for the rational design of high-performance electrocatalysts. *Small* **2019**, 190284–5.
- (13) Blanco-Brieva, G.; de Frutos Escrig, M. P.; Campos-Martin, J. M.; Fierro, J. L. Direct synthesis of hydrogen peroxide on palladium catalyst supported on sulfonic acid-functionalized silica. *Green Chem.* **2010**, 12, 1163–1166.
- (14) Pritchard, J. C.; He, Q.; Ntainjua, E. N.; Piccinini, M.; Edwards, J. K.; Herzing, A. A.; Carley, A. F.; Moulijn, J. A.; Kiely, C. J.; Hutchings, G. J. The effect of catalyst preparation method on the performance of supported Au–Pd catalysts for the direct synthesis of hydrogen peroxide. *Green Chem.* **2010**, 12, 915–921.
- (15) Xia, C.; Xia, Y.; Zhu, P.; Fan, L.; Wang, H. Direct electrosynthesis of pure aqueous H₂O₂ solutions up to 20% by weight using a solid electrolyte. *Science* **2019**, 366, 226–231.
- (16) Isaka, Y.; Oyama, K.; Yamada, Y.; Suenobu, T.; Fukuzumi, S. Photocatalytic production of hydrogen peroxide from water and dioxygen using cyano-bridged polynuclear transition metal complexes as water oxidation catalysts. *Catal. Sci. Technol.* **2016**, 6, 681–684.
- (17) Weng, B.; Wu, J.; Zhang, N.; Xu, Y. J. Observing the role of graphene in boosting the two-electron reduction of oxygen in graphene-WO₃ nanorod photocatalysts. *Langmuir* **2014**, 30, 5574–5584.
- (18) Siahrostami, S.; Verdager-Casadevall, A.; Karamad, M.; Deiana, D.; Malacrida, P.; Wickman, B.; Escudero-Escribano, M.; Paoli, E. A.; Frydendal, R.; Hansen, T. W. Enabling direct H₂O₂ production through rational electrocatalyst design. *Nat. mater.* **2013**, 12, 1137–1143.
- (19) Aveiro, L. R.; da Silva, A. G.; Antonin, V. S.; Candido, E. G.; Parreira, L. S.; Geonmonond, R. S.; de Freitas, I. C.; Lanza, M. R.; Camargo, P. H.; Santos, M. C. Carbon-supported MnO₂ nanoflowers: introducing oxygen vacancies for optimized volcano-type electrocatalytic activities towards H₂O₂ generation. *Electrochim. Acta* **2018**, 268, 101–110.
- (20) Cheng, F.; Su, Y.; Liang, J.; Tao, Z.; Chen, J. MnO₂-based nanostructures as catalysts for electrochemical oxygen reduction in alkaline media. *Chem. Mater.* **2010**, 22, 898–905.
- (21) Liang, Y.; Li, Y.; Wang, H.; Zhou, J.; Wang, J.; Regier, T.; Dai, H. Co₃O₄ nanocrystals on graphene as a synergistic catalyst for oxygen reduction reaction. *Nat. Mater.* **2011**, 10, 780–786.
- (22) Moraes, A.; Assumpção, M.; Papai, R.; Gaubeur, I.; Rocha, R. D. S.; Reis, R.; Calegaro, M. L.; Lanza, M. R. D. V.; Santos, M. C. D. Use of a vanadium nanostructured material for hydrogen peroxide electrogeneration. *J. Electroanal. Chem.* **2014**, 719, 127–132.

- (23) Ye, Y.; Kuai, L.; Geng, B. A template-free route to a Fe₃O₄-Co₃O₄ yolk-shell nanostructure as a noble-metal free electrocatalyst for ORR in alkaline media. *J. Mater. Chem.* **2012**, 22, 19132–19138.
- (24) Xu, A.; Han, W.; Li, J.; Sun, X.; Shen, J.; Wang, L. Electrogeneration of hydrogen peroxide using Ti/IrO₂-Ta₂O₅ anode in dual tubular membranes electro-Fenton reactor for the degradation of tricyclazole without aeration. *Chem. Eng. J.* **2016**, 295, 152–159.
- (25) Barros, W. R.; Wei, Q.; Zhang, G.; Sun, S.; Lanza, M. R.; Tavares, A. C. Oxygen reduction to hydrogen peroxide on Fe₃O₄ nanoparticles supported on printex carbon and graphene. *Electrochim. Acta* **2015**, 162, 263–270.
- (26) Carneiro, J. F.; Rocha, R. S.; Hammer, P.; Bertazzoli, R.; Lanza, M. Hydrogen peroxide electrogeneration in gas diffusion electrode nanostructured with Ta₂O₅. *Appl. Catal. A-Gen.* **2016**, 517, 161–167.
- (27) Oh, T.; Kim, J. Y.; Shin, Y.; Engelhard, M.; Weil, K. S. Effects of tungsten oxide addition on the electrochemical performance of nanoscale tantalum oxide-based electrocatalysts for proton exchange membrane (pem) fuel cells. *J. Power Sources* **2011**, 196, 6099–6103.
- (28) Chisaka, M.; Ishihara, A.; Suito, K.; Ota, K. I.; Muramoto, H. Oxygen reduction reaction activity of nitrogen-doped titanium oxide in acid media. *Electrochim. Acta* **2013**, 88, 697–707.
- (29) Kim, J. Y.; Oh, T. K.; Shin, Y.; Bonnett, J.; Weil, K. S. A novel non-platinum group electrocatalyst for pem fuel cell application. *Int. J. Hydrogen Energy* **2011**, 36, 4557–4564.
- (30) Assumpção, M. H. M. T.; Moraes, A.; De Souza, R.; Calegari, M.; Lanza, M.; Leite, E.; Cordeiro, M.; Hammer, P.; Santos, M. C. D. Influence of the preparation method and the support on H₂O₂ electrogeneration using cerium oxide nanoparticles. *Electrochim. Acta* **2013**, 111, 339–343.
- (31) Carneiro, J. F.; Paulo, M. J.; Siaz, M.; Tavares, A. C.; Lanza, M. R. Nb₂O₅ nanoparticles supported on reduced graphene oxide sheets as electrocatalyst for the H₂O₂ electrogeneration. *J. Catal.* **2015**, 332, 51–61.
- (32) Carneiro, J. F.; Trevelin, L. C.; Lima, A. S.; Meloni, G. N.; Bertotti, M.; Hammer, P.; Bertazzoli, R.; Lanza, M. R. Synthesis and characterization of ZrO₂/C as electrocatalyst for oxygen reduction to H₂O₂. *Electrocatalysis* **2017**, 8, 189–195.
- (33) Li, Z.; Liu, J.; Li, J.; Shen, J. Template free synthesis of crystallized nanoporous F-Ta₂O₅ spheres for effective photocatalytic hydrogen production. *Nanoscale* **2012**, 4, 3867–70.
- (34) Lu, Z.; Chen, G.; Siahrostami, S.; Chen, Z.; Liu, K.; Xie, J.; Liao, L.; Wu, T.; Lin, D.; Liu, Y.; Jaramillo, T. F.; Nørskov, J. K.; Cui, Y. High-efficiency oxygen reduction to hydrogen peroxide catalysed by oxidized carbon materials. *Nat. Catal.* **2018**, 1, 156–162.
- (35) Yuan, D.; Wei, Z.; Han, P.; Yang, C.; Huang, L.; Gu, Z.; Ding, Y.; Ma, J.; Zheng, G. Electron distribution tuning of fluorine-doped carbon for ammonia electrosynthesis. *J. Mater. Chem. A* **2019**, 7, 16979–16983.
- (36) Guo, L.; He, H.; Ren, Y.; Wang, C.; Li, M. Core-shell SiO@ F-doped C composites with interspaces and voids as anodes for high-performance lithium-ion batteries. *Chem. Eng. J.* **2018**, 335, 32–40.
- (37) Li, Z.; Xu, J.; Wang, J.; Niu, D.; Hu, S.; Zhang, X. Well-dispersed amorphous Ta₂O₅ chemically grafted onto multi-walled carbon nanotubes for high-performance lithium sulfur battery. *Int. J. Electrochem. Sci* **2019**, 14, 6628–6642.
- (38) Yu, X.; Li, W.; Li, Z.; Liu, J.; Hu, P. Defect engineered Ta₂O₅ nanorod: one-pot synthesis, visible-light driven hydrogen generation and mechanism. *Appl. Catal. B-Environ.* **2017**, 217, 48–56.
- (39) Zhuang, Y.; Seong, J. G.; Do, Y. S.; Jo, H. J.; Cui, Z.; Lee, J.; Lee, Y. M.; Guiver, M. D. Intrinsically microporous soluble polyimides incorporating Tröger's base for membrane gas separation. *Macromolecules* **2014**, 47, 3254–3262.
- (40) Sun, Y.; Sinev, I.; Ju, W.; Bergmann, A.; Dresch, S.; Kühl, S.; Spoeri, C.; Schmies, H.; Wang, H.; Bernsmeier, D.; Paul, B.; Schmack, R.; Kraehnert, R.; Cuenya, B. R.; Strasser, P. Efficient electrochemical hydrogen peroxide production from molecular oxygen on nitrogen-doped mesoporous carbon catalysts. *ACS Catal.* **2018**, 8, 2844–2856.
- (41) Chen, S.; Chen, Z.; Siahrostami, S.; Higgins, D.; Nordlund, D.; Sokaras, D.; Kim, T. R.; Liu, Y.; Yan, X.; Nilsson, E. Designing boron nitride islands in carbon materials for efficient electrochemical synthesis of hydrogen peroxide. *J. Am. Chem. Soc.* **2018**, 140, 7851–7859.